Wideband Radar Cross Section Reduction of Slot Antennas Arrays

Simone Genovesi, *Member, IEEE*, Filippo Costa, *Member, IEEE*, and Agostino Monorchio, *Fellow, IEEE*

***Abstract*—A comprehensive analysis aimed at reducing the radar cross section (RCS) of array antennas, preserving at the same time their radiating performance, is presented. A microstrip slot array is considered as a test case to illustrate the proposed strategy for radar cross section reduction (RCSR). It is shown that a remarkable reduction of the radar signature can be accomplished over a frequency band as wide as two octaves by employing an array of periodic resistive elements in front of the radiating apertures. The monostatic and bistatic RCS of the proposed structures are investigated both for normal and oblique incidence. Different arrangements and geometries of the periodic resistive pattern are thoroughly analyzed showing the benefits and the drawbacks in terms of antenna gain and level of the scattered fields. Furthermore, the use of metallic parasitic elements for enhancing the antenna gain is considered, and the scattering phenomena caused by their presence are addressed, taking into account the appearance of grating lobes. The antenna designs are also analyzed by resorting to a bidimensional color plot presenting the variation of the reradiated field both in frequency and spatial domain. The guidelines illustrated by the proposed examples can be easily applied to other antenna architectures.**

***Index Terms*—Frequency selective surface (FSS), periodic resistive surface (PRS), radar absorbing materials (RAMs), radar cross section reduction (RCSR), slot antennas array.**

I. Introduction

THE level of the field backscattered from an object when hit by an electromagnetic wave is an important parameter in a wide range of applications. For example, in the context of radio-frequency identification (RFID), the modulated backscattering operated by the chip is of utmost importance in recovering the information provided by the tag placed in the interrogated item [1] and the level of reradiated energy is such a desirable feature that a great effort is devoted towards its enhancement. However, in other situations, the electromagnetic echo is an undesired side effect which has fostered during recent decades a research aimed to consistently reduce it [2], [3]. This last scenario may refer to a radar target, such as an unmanned combat aerial vehicle (UCAV) or a warship, for which low observability is an imperative feature. In this framework, the radar cross section (RCS) provides a meaningful description of the energy backscattered by the object.

A well-known technique adopted for decreasing the RCS of aircrafts or other bulky platforms consists of shaping the object surfaces in order to reflect the scattered energy away from the detecting receiver. However, one of the main obstacles in achieving the radar cross section reduction (RCSR) is determined by the presence of an antenna on the target [4]. Sometimes an antenna can be tilted or have its shape modified to deflect the probing wave, so causing the strongest reflection at directions where the RCS is less significant than at others, typically out of the broadside [5]–[7]. A similar objective can also be accomplished by employing a bandpass frequency-selective surfaces (FSS) radome that, being totally reflecting, deviates elsewhere the interrogating waves outside the antenna operating band [8]. Moreover, FSSs can be employed as a frequency-selective ground plane to reduce the RCS of a reflectarray [9], an array of monopoles [10], or even printed microstrip patch arrays [11]. The FSS role in the latter group of FSS designs is to provide a perfect electric ground plane within the working bandwidth of the radiating device while exhibiting pass-band characteristics at other frequency bands, thus being transparent to the impinging wave. In the aforementioned cases, the purpose is to forbid the energy from coming back to the detecting device, thus achieving a monostatic RCS reduction and avoiding the target localization.

However, it may happen in some cases that the antenna structure cannot be easily altered without resorting to a complete redesign. Moreover, shaping is not so effective in the case of bistatic radars [12], [13]. In this case, a different approach can be followed for pursuing the reduction of the scattered energy by absorbing the impinging wave. It relies on the use of radar absorbing materials (RAMs) [14], [15], which transform the radio frequency energy into heat. Recently, printed resistive periodic structures have been successfully explored to dissipate the energy impinging on an antenna array [16], [17] or radome [18], whereas other implementations involved tapered resistive sheets [19], [20]. Nevertheless, to the best of our knowledge, most of the proposed configurations provide the RCS reduction in a limited frequency bandwidth. Up to now, very few papers exploiting RAM to perform wideband RCS reduction of antenna arrays have been published, and a comprehensive study of this approach is not available.

The aim of this work is to provide a study to illustrate the benefits and drawbacks of employing a suitable superstrate based on periodic resistive surfaces (PRS) for obtaining a wideband RCSR of a microstrip array of slot antennas. The attention is focused on this case-study array, and the effects of different periodic surface designs on the performance of the radiating struc-

Manuscript received May 05, 2012; revised August 27, 2013; accepted September 19, 2013. Date of publication October 30, 2013; date of current version December 31, 2013.

The authors are with the Dipartimento di Ingegneria dell'Informazione, University of Pisa, Pisa 56122, Italy, and with RaSS National Laboratory, CNIT Galleria, Pisa 56124, Italy (e-mail: simone.genovesi@iet.unipi.it; filippo.costa@iet.unipi.it; a.monorchio@ieee.org).

Color versions of one or more of the figures in this paper are available online at http://ieeexplore.ieee.org.

Digital Object Identifier 10.1109/TAP.2013.2287888

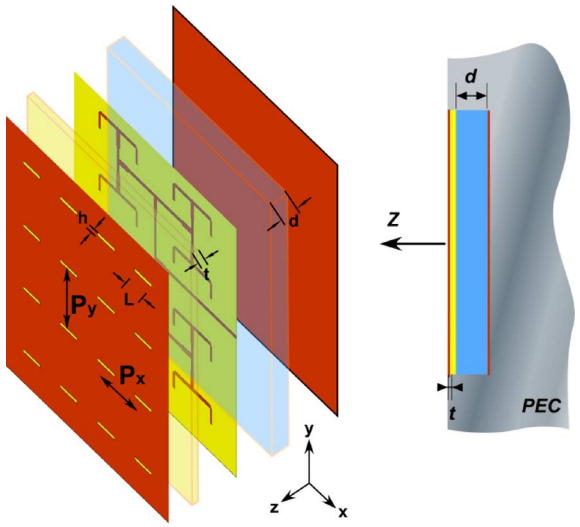

(a) (b)

Fig. 1. Original 4 × 4 microstrip slot antenna array: *(a)* exploded view of the array with metallized borders removed and *(b)* array integrated into a PEC object.

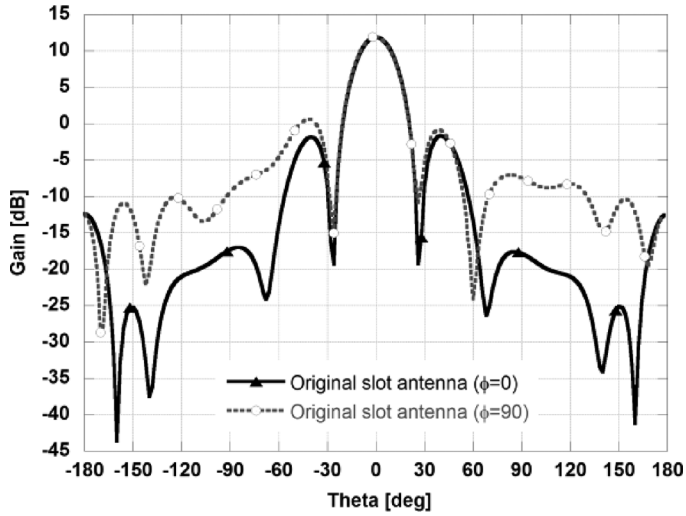

Fig. 2. Radiation pattern of the 4 × 4 microstrip slot antenna on $\phi = 0°$ plane and $\phi = 90°$ plane at 2.5 GHz.

ture are addressed. In particular, the reduction of the radar signature for normal and oblique plane wave incidence is considered, as well as the effect on the antenna gain.

The paper is organized as follows. A radiating device comprising a 4 × 4 periodic arrangement of microstrip slot antennas is described in Section II. In Section III, the frequency response of the wideband periodic resistive surface is characterized, and a physical interpretation of the interaction between a normal impinging electromagnetic wave and the planar radar absorbing material is provided by resorting to a transmission line model. Section IV addresses the reduction of RCS exhibited by the proposed superstrates and the degradation of the radiating performance obtained by employing the different configurations of the periodic resistive surface in the case of normal incidence. Further considerations useful to understand the effects of the proposed superstrates on the RCSR behavior are provided in Section V by using a comprehensive map of the total scattered power. Since the RCS is a strongly angular-dependent property of the target, additional elements useful to the designer for finding the most suitable tradeoff are provided in Section VI where the RCSRs exhibited by some of the proposed designs are analyzed also for oblique incidence for both monostatic and bistatic case. Finally, concluding remarks are drawn in Section VI.

II. Microstrip Slot Antenna Array

The reference array of 4 × 4 slots is shown in Fig. 1(a). It operates within the frequency bandwidth 2.43–2.53 GHz. Each slot is etched on the top conductive surface of a FR4 dielectric slab ($\varepsilon_r = 4.4$, $\mathrm{tg}\delta = 0.025$) with thickness $t = 1.6$ mm. A possible operative scenario is illustrated in Fig. 1(b), where the array is installed inside a metallic object.

The bottom surface hosts the corporate feed network, which excites every single aperture. The feeding network is enclosed within a metallized cavity in order to prevent undesired back radiation, and the thickness d of the Rohacell substrate is 1.5 cm. The periodicity of the slot distribution along x is equal to $P_x = 6.4$ cm, whereas on the y-axis, it is $P_y = 6.4$ cm. The slot width L and height h are equal to 2.9 and 0.3 cm, respectively. The overall dimension of the antenna in the xy plane is 28 cm × 26 cm. The gain on the principal planes is reported in Fig. 2 at 2.5 GHz. The antenna exhibits a maximum gain of 11.9 dB (11.4 dB higher than the peak side lobe level), and an HPBW of 28°. It is worth emphasizing that the maximum gain may be higher if a low-loss substrate would be employed for the feeding network.

From a scattering point of view, it is important to notice that, as in the case of a single antenna, the RCS of an array can be considered composed by an antenna component and by a structural term [21]–[24]:

$$\sigma = \left| \sqrt{\sigma_{\mathrm{structural}}} - (1 - \Gamma_a) \sqrt{\sigma_{\mathrm{antenna}}} e^{j\phi} \right|^2$$

where σ is the total RCS of the target, $\sigma_{\mathrm{structural}}$ is related to the field scattered by the short-circuited antenna, $\sigma_{\mathrm{antenna}}$ represents the field scattered by the antenna which involves the value of the port impedance, Γ_a is the antenna reflection coefficient, and ϕ is the relative phase between the two terms. Our goal consists of reducing the structural term $\sigma_{\mathrm{structural}}$ of an antenna array, and it will be studied under the short circuit condition of the feeding port.

The monostatic RCS due to an orthogonal impinging plane wave with a direction of propagation along z axis is shown in Fig. 3. The RCS has a monotonically increasing behavior as expected, always higher than 10 dB after 4.0 GHz. The result is confirmed by physical optics and it is apparent that the impinging wave is coupled to the slots only for TM polarization. All the simulations have been performed by using CST Microwave Studio [25].

Finally, to address the effect of the antenna component, we have evaluated again the monostatic RCS but with a 50-Ω load at the feeding port (Fig. 4). The only relevant RCS variation is observed around the fundamental working frequency of the antenna; therefore, we can consider the antenna component a negligible high-order RCS perturbation out of the working bandwidth.

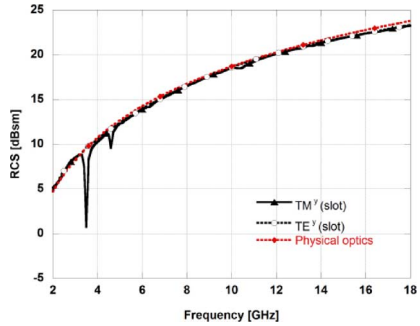

Fig. 3. Monostatic RCS of the 4×4 microstrip slot antenna array for a normally impinging plane wave with TE^y and TM^y polarization. Physical optics result is also shown.

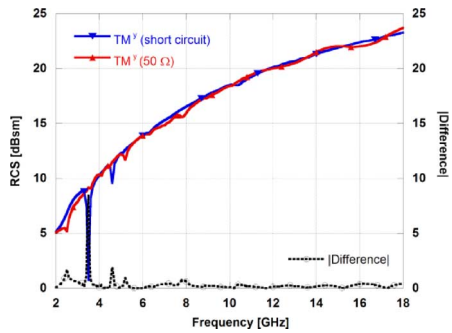

Fig. 4. Comparison between the monostatic RCS of the original slot antenna in the case the source is closed on a short circuit and on a 50-Ω load. The magnitude of the difference is shown as well.

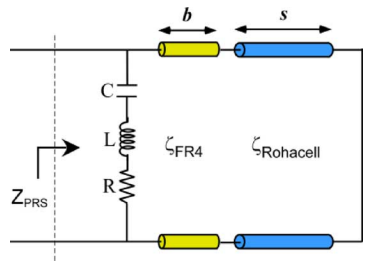

Fig. 5. Equivalent transmission line model of the considered uniform PRS.

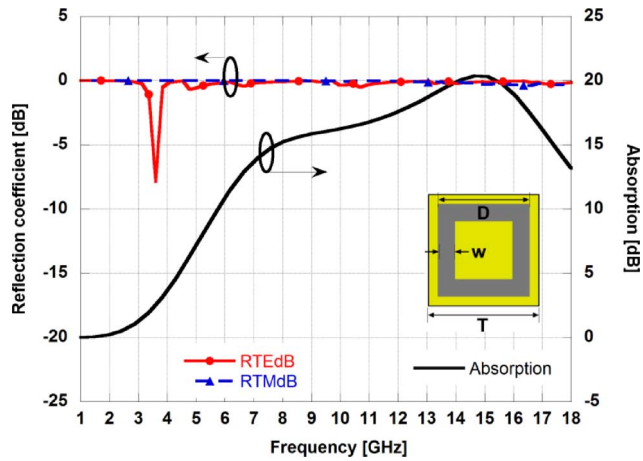

Fig. 6. Frequency response of an infinite array of slots is shown for an impinging TE^y plane wave (RTE) as well as for a TE^y one (RTM). Absorption of the infinite PRS printed on a fully grounded dielectric slab is also illustrated. The unit cell of the uniform PRS is shown in the inset.

III. Low Radar Cross Section Array by Employing a Periodic Resistive Surface

Differently from previous works aimed to a narrow-band absorption of the impinging wave by exploiting periodic lossy surfaces [12], [16], we focus our attention on a wideband RCSR. The analysis we propose has a twofold objective: it is our interest to obtain a robust RCSR in the widest possible bandwidth, but, at the same time, we also intend to maximize achievable gain. For this reason, we investigate six different configurations with the aim to select the best tradeoff between RCS reduction and antenna performance.

First of all, we observe that the metallic surface hosting the slots completely reflects a normally impinging plane wave within the bandwidth 4.0–18.0 GHz (Fig. 6). This means that the slotted surface acts like a continuous metallic plane for both TE and TM polarization, and thus it can be exploited in this bandwidth as a ground plane for designing an absorber by using a suitable periodic resistive surface in front of it. In our test case, the periodic resistive surface is printed, for manufacturing purposes, on a thin FR4 dielectric substrate (thickness $b = 0.02$ cm), and it is placed at a proper distance s from the slotted surface acting as a solid ground plane. A periodic surface can be advantageously described by an equivalent transmission line model [26]–[28] where the uniform PRS can be modeled as a series comprising the resistance R, an inductance L, and a capacitance C, the FR4 and Rohacell substrates as transmission lines and the ground plane as a short circuit (Fig. 5). The input impedance Z_{ABS} includes the effect of both the dielectric substrate and the Rohacell spacer d with propagation constant ζ_{FR4} and ζ_{air} , respectively. The impedance Z_{ABS} depends on the shape and periodicity of the patterned surface, the employed resistive materials, and dielectric substrates [29]. In order to synthesize a perfect absorber, the input impedance Z_{ABS} has to match the free space one (377 Ω) even if nearby values can guarantee an acceptable level of radar absorption as well.

On the basis of our former studies [26], [29], we have selected the square loop element reported in the inset of Fig. 6 as a promising PRS candidate. The frequency response of the absorptive surface depends on the unit cell periodicity T, pattern shape (ring side D, and ring width w), and the resistance of the ring surface R. In order to make the design feasible, we have imposed the unit cell periodicity and the slot periodicity to be commensurable. Our purpose is to achieve a low-radar observability within the C band (4.0–8.0 GHz), X band (8.0–12.0 GHz), and Ku band (12.0–18.0 GHz) that are widely used by many acquisition systems. The absorption coefficient of the optimized uniform PRS is shown in Fig. 6 for the following values of the FSS parameters: $D = 1.1$ cm, $T = 1.28$ cm, $w = 0.24$ cm, $s = 0.5$ cm, and $R = 75\ \Omega/\mathrm{sq}$.

The initial and most intuitive low-RCS design of the microstrip slot antenna array employs a finite uniform PRS comprising 20×20 unit cells. The overall structure with the superstrate hosting the optimized uniform PRS is shown in Fig. 7. The S_{11} parameter of the antenna array is shifted upward as a consequence of the resistive superstrate (Fig. 8), but a good match is preserved for both configurations at 2.5 GHz, which will be

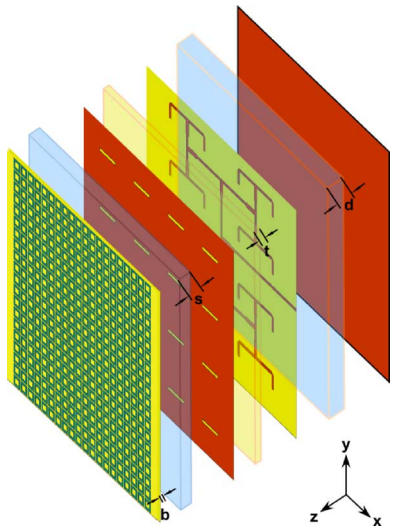

Fig. 7. Exploded view of the original 4 × 4 microstrip slot antenna array with the superstrate hosting the uniform PRS placed at distance s from the slotted conductive plane (metallized borders removed).

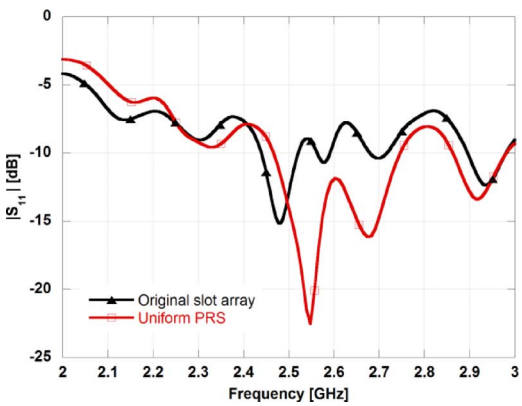

Fig. 8. S_{11} parameter of the original 4 × 4 microstrip slot antenna and with the uniform PRS superstrate.

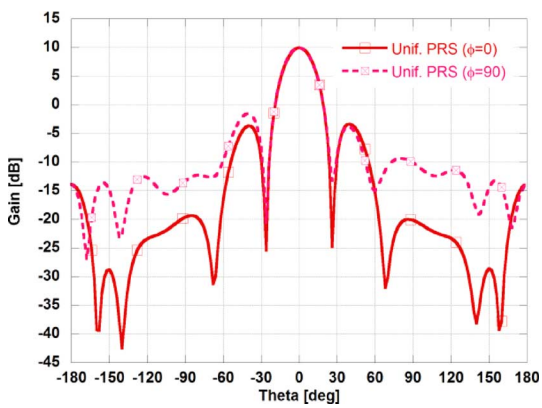

Fig. 9. Radiation pattern of the 4 × 4 microstrip slot antenna with the uniform PRS superstrate on $\phi = 0°$ plane and $\phi = 90°$ plane at 2.5 GHz.

considered as a reference frequency for all the following comparisons involving the antenna gain. Fig. 9 reports the radiation patterns of the array on E and H planes at 2.5 GHz. By comparing the variation of the gain level with respect to the previous

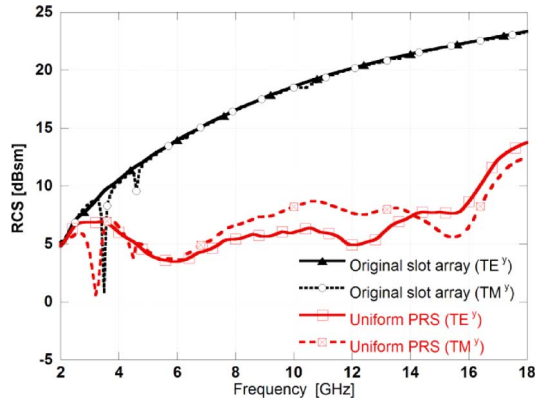

Fig. 10. Monostatic RCS of the 4 × 4 microstrip slot antenna array with the uniform PRS superstrate for a normally impinging plane wave with TE^y polarization and TM^y polarization.

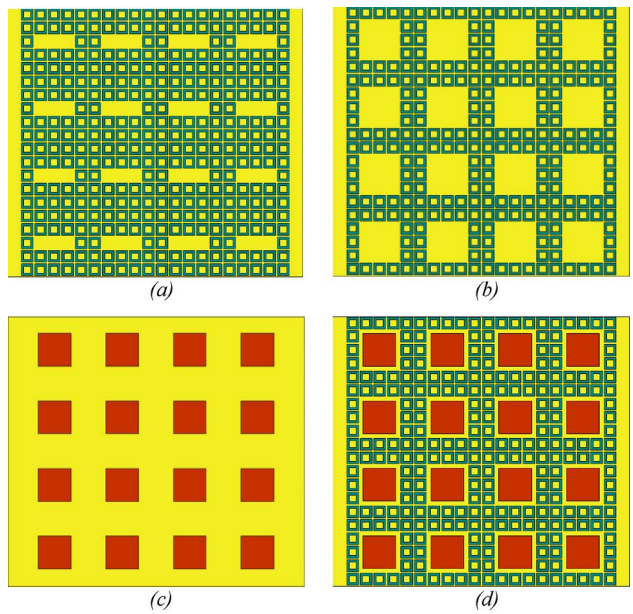

Fig. 11. Superstrates placed in front of the original microstrip slot array antenna. The four represented configurations are *(a) Conf#3*, with some unit cells removed in correspondence of the underneath slots, *(b) Conf#4*, with more unit cells removed, *(c) Conf#5*, with a layer with only parasitic patches, and *(d) Conf#6*, with the PRS around parasitic patches.

results, it is apparent that maximum gain diminishes to 9.9 dB, that is, 2.0 dB less than the original one. On the other hand, the absorbing structure allows a noticeable RCSR between 4 and 18 GHz, as observed in Fig. 10, where the monostatic RCS is shown.

IV. Best Trade-Off Between Radar Cross Section Reduction and Radiation Performance

The RCSR of an array is a compromise between the achieved level of radar invisibility and the increased system complexity or the degradation of radiating performance. Both these aspects have been taken into account in order to find the best tradeoff array configuration. To this aim, four additional configurations of the superstrate have been investigated and their performance compared (Fig. 11).

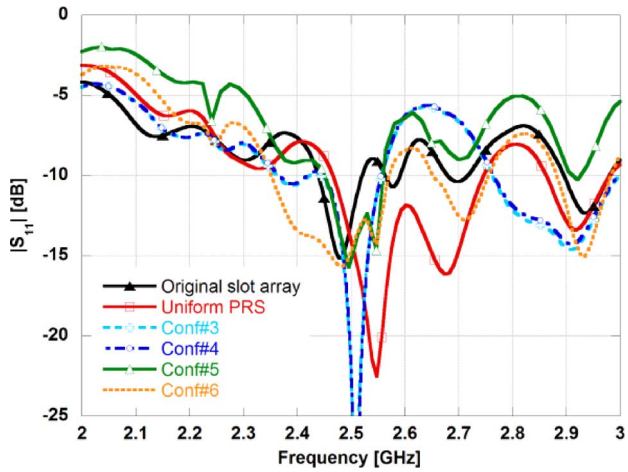

Fig. 12. Comparison among the S_{11} parameters of each array.

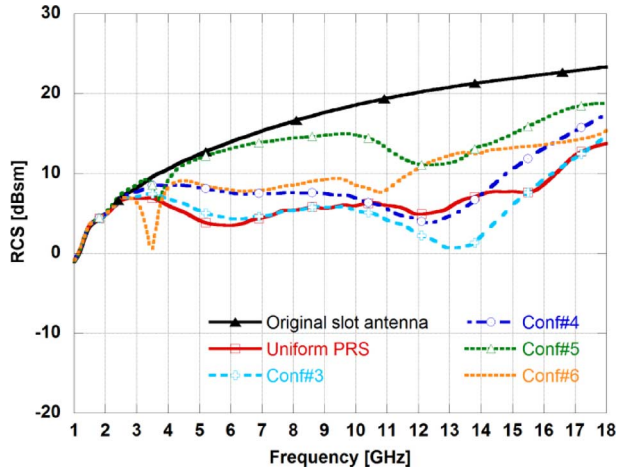

Fig. 14. Monostatic RCS of the investigated arrays for a normally impinging plane wave with TE^y polarization.

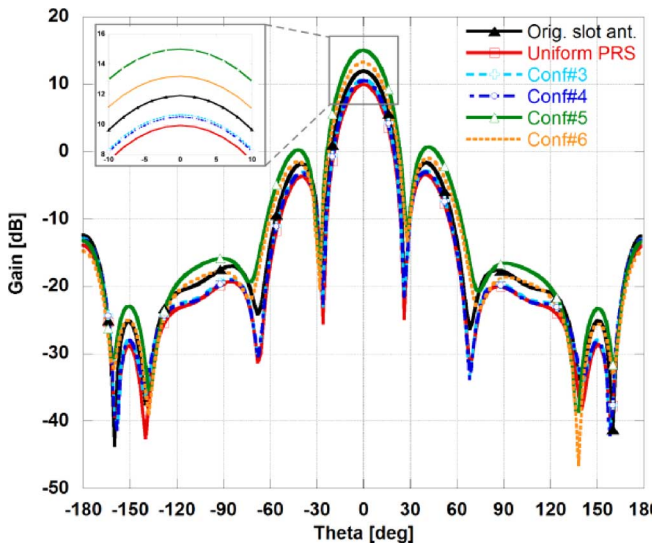

Fig. 13. Comparison among the gain pattern on $\phi = hbox0^\circ$ plane.

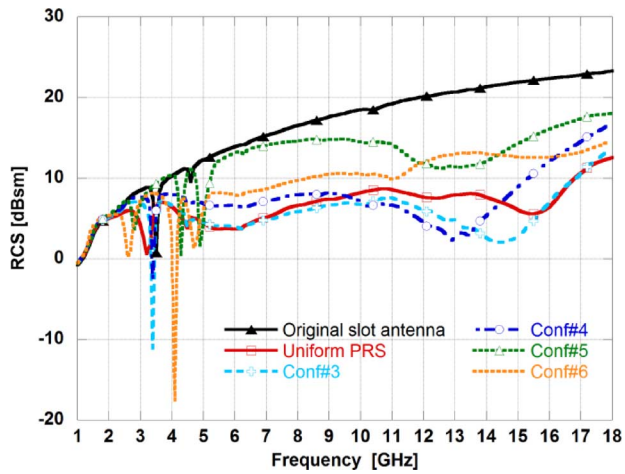

Fig. 15. Monostatic RCS of the investigated arrays for a normally impinging plane wave with TM^y polarization.

The first modified design (*Conf#3*) is characterized by the removal of three lossy unit cells for each underneath slot (Fig. 11(a)) to achieve a lower gain degradation than the uniform PRS. In order to further reduce the impact of the lossy surface on the antenna gain, an additional setup (*Conf#4*) with a lower number of resistive unit cells centered in front of the radiating slots has been considered (Fig. 11(b)). In addition, we have considered an alternative configuration, including a parasitic patch accommodated upon the slots in order to improve the antenna radiation properties. The latter is reported in Fig. 11(c) (*Conf#5*) besides its corresponding low-RCS design (*Conf#6*), where the parasitic patches are surrounded by the PRS. All the modified antennas work around 2.5 GHz, as shown in Fig. 12.

The comparison among the gain achieved on the plane $\phi = 0^\circ$ is reported in Fig. 13. The level of RCSR offered by each configuration with respect to the original slot array is illustrated in Figs. 14 and 15 both for TE and TM polarization. As expected, the highest gain is reached by *Conf#5* configuration (15 dB) because of the presence of parasitic patches. The low-RCS design comprising resistive unit cells around the parasitic patch (*Conf#6*) shows a gain of 13.2 dB, which is higher than the initial configuration (11.9 dB) reported in Section II.

Let us now consider the antenna configuration without parasitic patches. In this case, the removal of some of the resistive rings, i.e., *Conf#3* (10.6 dB) and *Conf#4* (10.5 dB), mitigates the gain reduction with respect to the uniform PRS configuration (9.9 dB) and as a consequence the efficiency is improved ($\eta_{Conf\#3} = -2.8$ dB, $\eta_{Conf\#4} = -2.9$ dB, whereas $\eta_{\mathrm{PRS}} = -3.5$ dB).

By inspecting the RCSR for both TE^y and TM^y polarization shown in Fig. 14, it is apparent that all the analyzed configurations exhibit a lower radar signature than the original microstrip slot array (up to 20 dB of RCSR for *Conf#3* and *Conf#4*). A summary of the superstrates performance for a normally impinging plane wave is reported in Table I in terms of the maximum gain at 2.5 GHz and the average (arithmetic mean) monostatic RCS over the two-octave bandwidth 4.0–18 GHz. In order to provide a more comprehensive analysis of the proposed RCSR

TABLE I
SUMMARY OF THE DIFFERENT SUPERSTRATES PERFORMANCE

	Avg RCS [dBsm]	Max gain [dB]
Original array	18.6 (poor)	11.9 (good)
Uniform PRS	6.6 (very good)	9.9 (poor)
Conf#3	5.6 (very good)	10.6 (fair)
Conf#4	8.5 (good)	10.5 (fair)
Conf#5	14.0 (poor)	15 (very good)
Conf#6	10.5 (fair)	13.2 (good)

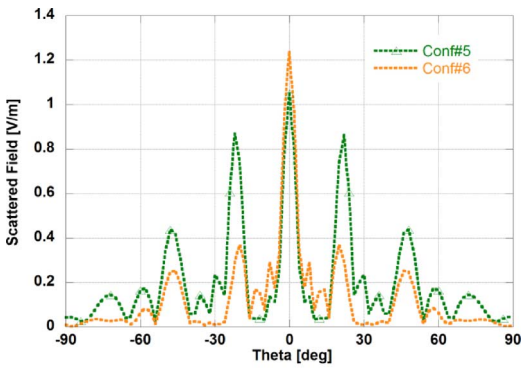

(a)

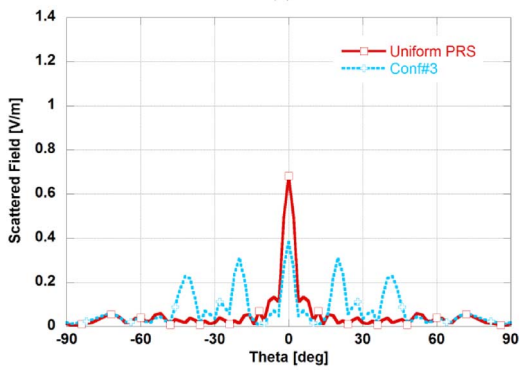

(b)

Fig. 16. Comparison among the TM^y scattered field on $\phi = 0°$ plane for (a) *Conf#5* and *Conf#6* configurations at 13 GHz and (b) uniform PRS and *Conf#3* configurations at 14 GHz.

strategy, the performances of the superstrates are also studied for an oblique incidence plane wave and the bistatic case.

V. EFFECT OF GRATING LOBES ON THE RCSR

We now examine some meaningful phenomena observed in the RCS curves shown in Figs. 14 and 15. Let us observe the RCS curves obtained for *Conf#5* design, which has no resistive surface in the superstrate. It is evident that it exhibits a level of RCS lower than *Conf#6* around 13 GHz for both polarizations. A similar phenomenon is observed at 14 GHz, where the original slot array with the uniform PRS superstrate determines a higher radar signature than *Conf#3* or *Conf#4*, which have their periodicity altered by the removal of some resistive unit cells located in front of the radiating slots. In order to get a better understanding of the involved phenomena, the scattered fields of *Conf#5* and *Conf#6* configurations at 13.0 GHz (Fig. 16(a)) and the scattered field of uniform PRS and *Conf#3* at 14 GHz (Fig. 16(b)) are compared on the plane $\phi = 0$ for TM^y.

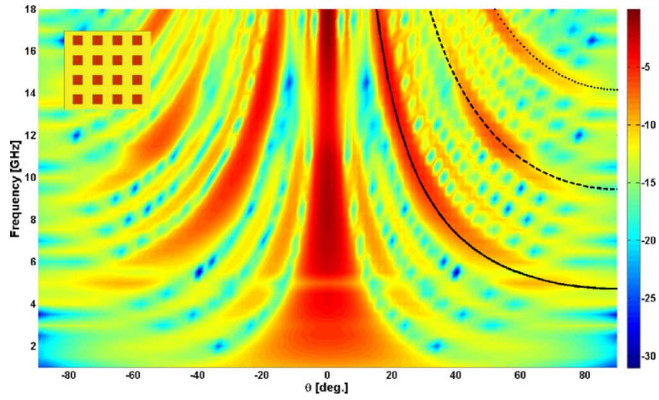

(a)

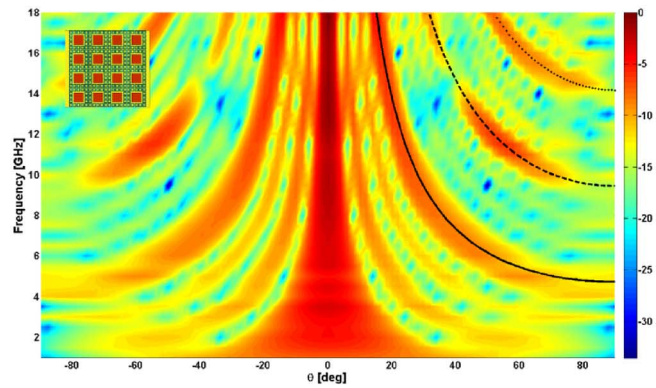

(b)

Fig. 17. Normalized scattered field for an impinging TM^y plane wave ($\theta = 0°$) in the case of *(a)* the *Conf#5* configuration and *(b)* the *Conf#6* configuration. Grating lobe for $n = 1, 2, 3$ are plotted with continuous, dashed, and dotted lines, respectively. Front view of each superstrate is shown in the inset. Each plot is normalized to its maximum value: *(a)* 18 dBsm and *(b)* 14.5 dBsm.

It is apparent that only close to the monostatic direction ($\theta = 0°$), the scattered field of *Conf#6* and uniform PRS is slightly higher than *Conf#5* and *Conf#3*, respectively. Out of the solid angle (approximately 32°), the RCS of *Conf#6* and uniform PRS is substantially reduced because of the presence of the absorbing materials. In order to visualize both the frequency and the angle behavior of the RCS in the same chart, we adopted a plot reporting the normalized scattered field variations both in frequency and angle for an impinging plane wave orthogonal to the array ($\theta = 0°$).

The bidimensional plots concerning the four analyzed cases (uniform PRS, *Conf#3*, *Conf#5*, *Conf #6*) are shown in Figs. 17 and 18. Each plot is normalized with respect to the maximum value of the scattered field within the considered frequency and angular intervals. It is clear from the color plot reported in Fig. 17(a) for the *Conf #5* () that a strong scattering starts around 4.7 GHz at angles grazing the array surfaces and then converges toward the orthogonal direction without reaching it. Other strong contributions come into play at around 9.4 and 13.75 GHz. This is due to the onset of grating lobes related to the periodicity of the parasitic patches. In fact, if we consider the periodicity P_x of the parasitic patches in the superstrate and the slots engraved on the ground plane and we use

$$f_{\mathrm{GL}_n} = \frac{n\,c}{P_x\,(\sin\theta + 1)} \tag{1}$$

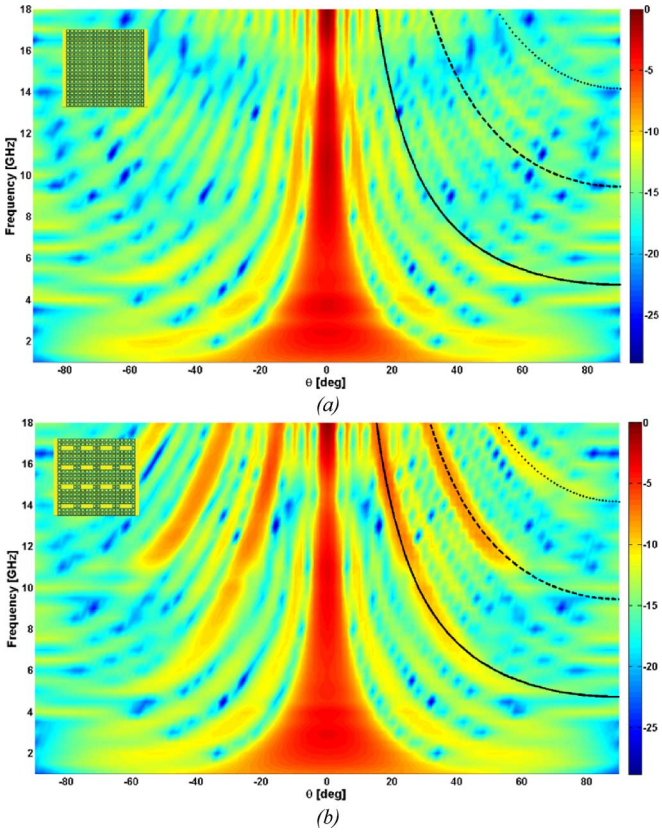

Fig. 18. Normalized scattered field for an impinging TM^y plane wave ($\theta = 0^\circ$) in the case of *(a)* the uniform PRS case and *(b)* the *Conf#3* configuration. Grating lobe for $n = 1, 2, 3$ are plotted with continuous, dashed, and dotted lines, respectively. Front view of each superstrate is shown in the inset. Each plot is normalized to its maximum value: *(a)* 12.5 dBsm and *(b)* 13.7 dBsm.

with c being the speed of light and $f_{\mathrm{GL}n}$ is the lowest frequency where the grating lobe of order n appears for a plane wave incident from an angle θ [8], we find a good agreement with the three aforementioned frequencies ($f_{\mathrm{GL1}} = 4.68$ GHz, $f_{\mathrm{GL2}} = 9.375$ GHz, $f_{\mathrm{GL3}} = 14.04$ GHz). Similar considerations can be drawn by inspecting the plot in Fig. 17(b) for the *Conf#6* superstrate, which exhibits the same off-normal spreading of the reradiated energy. By observing Fig. 17(a) and (b), we may infer that the *Conf#5* configuration has a lower monostatic RCS than the *Conf#6* at 13 GHz because it redirects more energy toward grating lobes directions.

The connection between P_x and the grating lobes occurrence becomes more meaningful if the plots of uniform PRS and Conf#3 displayed in Fig. 18 are considered.

In the former case (Fig. 18(a)), all the superstrate is composed by resistive unit cells, and the grating lobes are absent since their periodicity T avoids the onset of grating lobes in this frequency range for normal incidence. On the contrary, in the *Conf#3* case (Fig. 18(b)), the unit cell periodicity of the periodic resistive surface T is broken by the removed rings and the grating lobes that depend on the array periodicity P_x appear again. Therefore, the effect of parasitic elements in the superstrate has to be taken into account to predict directions of higher bistatic RCS, which are absent in the uniform periodic surface.

As already pointed out, all the previous plots have been normalized to their own RCS maximum value to provide a clear

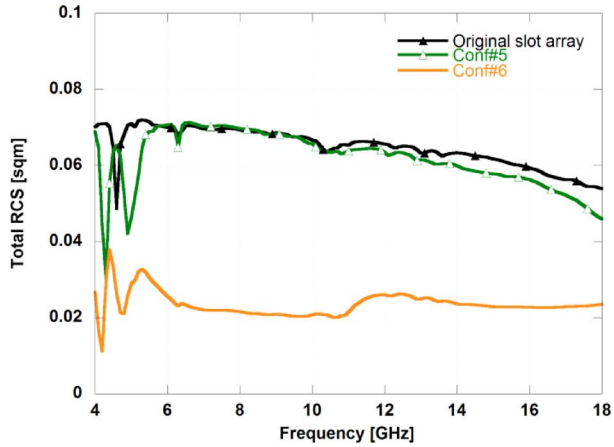

Fig. 19. Comparison between the total RCS in the case of *Conf#5* and *Conf#6* configurations for an impinging TM^y plane wave ($\theta = 0^\circ$).

description of the reradiated energy spreading (the same color does not represent the same absolute value). This normalization may affect the comparison between two configurations. One may question, for example, if *Conf#5* is more effective than *Conf#6* in diminishing the electromagnetic echo at 13 GHz. Similar questions may be raised for the other examples. In order to synthesize the performance of the low-RCS antennas over all angles, we have evaluated the total RCS σ_{T} defined as [30]

$$\sigma_{\mathrm{T}} = \frac{1}{4\pi} \iint \sigma(\theta, \phi) \sin\theta d\theta d\phi \tag{2}$$

evaluated toward the interrogating source ($-90^\circ \le \phi \le 90^\circ$ and $-90^\circ \le \theta \le 90^\circ$ and considering an impinging plane wave with electric field amplitude equal to 1 V/m to undoubtedly verify the usefulness of the presented configurations in reducing the radar signature. In Fig. 19, the comparison between the total RCS by the antenna array with parasitic patches in the presence and absence of the surrounding resistive elements is reported. It is apparent that *Conf#6* always scatters less power than its corresponding structure without resistive rings (*Conf#5*).

A similar consideration can be drawn looking at Fig. 20 where the absorption of uniform PRS and *Conf#3* are both better than the one of the original slot array.

VI. RCSR at Oblique Incidence

To examine the effectiveness of using a RAM in diminishing the electromagnetic echo of the array antenna, we consider the case of an oblique-impinging TM^y plane wave. In particular, a comparison between the original slot array and the *Conf#6* is done in terms of the bistatic RCS (specular) as well as the overall scattered energy. Moreover, the case of monostatic RCS at oblique incidence is evaluated in more detail for the following configurations: original slot array, uniform PRS case, *Conf#5*, and *Conf#6*.

A. Bistatic Radar Cross Section and Scattered Energy

The bistatic RCS and the scattered energy from two different directions, namely *Oblique#1* ($\theta = 30^\circ$, $\phi = 0^\circ$) and *Oblique #2* ($\theta = 60$, $\phi = 0$), are addressed for *Conf#6* since it is a good tradeoff between RCSR and radiating performance. The results

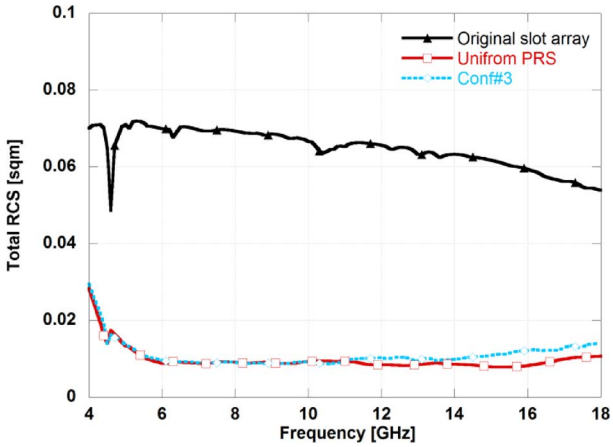

Fig. 20. Comparison between the total RCS in the case of uniform PRS and *Conf#3* configurations for an impinging TM^y plane wave ($\theta = 0°$).

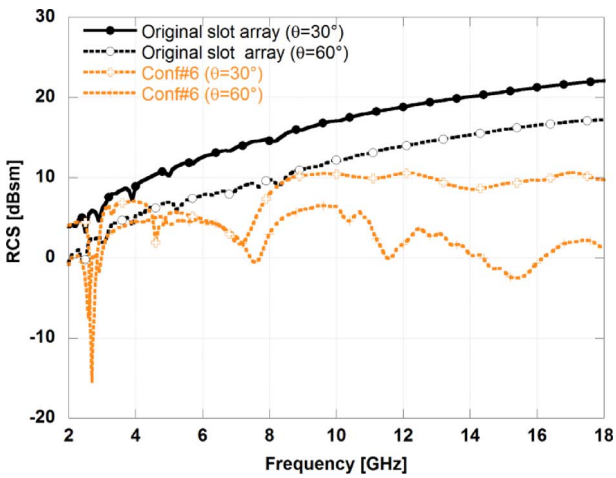

Fig. 21. Comparison between the bistatic RCS of the investigated arrays for an oblique impinging plane wave with TM^y polarization ($\theta = 30°$ or $\theta = 60$, $\phi = 180°$).

are compared with the original slot array. First of all, the bistatic RCSs have been evaluated for an observer along the specular direction ($\theta = 60°$ or $\theta = 30°$, $\phi = 180°$), and they are shown in Fig. 21.

Next, the normalized scattered fields for case *Oblique#1* are illustrated for the original slot antenna as well as for *Conf#6* in Figs. 22 and 23, respectively. For the *Conf#6* structure, grating lobes related to the slot/patch periodicity P_x start to appear around 3.15, 6.29, 9.44, 12.6, and 15.74 GHz. This angle of incidence determines also the onset of grating lobes due to the periodicity T of the periodic resistive surface which emerge around 15.6 GHz (Fig. 23).

For the case *Oblique#2*, the comparison between the scattered energy for the aforementioned structures is summarized in Figs. 24 and 25, where it can be seen that the grating lobes determined by the slot/patch periodicity P_x emerge around 2.35, 5, 7.6, 10.1, and 12.65 GHz, whereas the one due to the periodicity T start around 12.56 GHz.

As reported for the case of normal incidence, in order to check the RCSR performance of the low-RCS antennas over all incidence angles, we have evaluated the energy scattered toward all

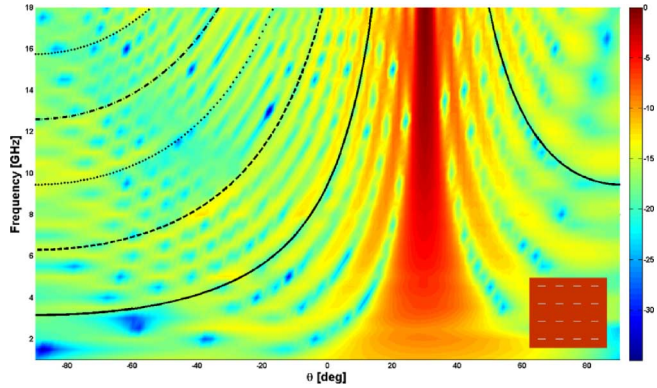

Fig. 22. Normalized scattered field for an impinging TM^y plane wave ($\theta = 30°$) for the original slot array. Grating lobes for $n = 1, 2, 3, 4, 5$ are plotted with continuous, dashed and dotted lines. Plot is normalized to its maximum value (22.1 dBsm).

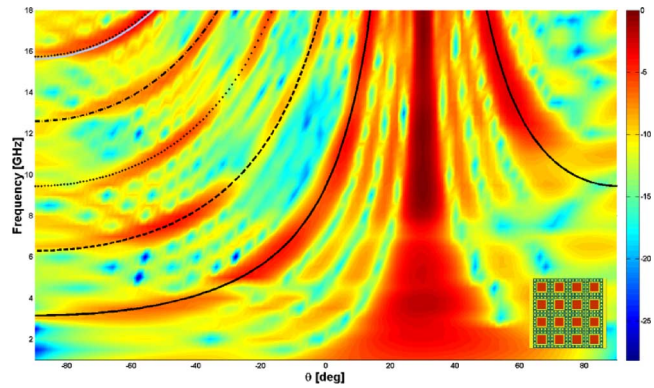

Fig. 23. Normalized scattered field for an impinging TM^y plane wave ($\theta = 30°$) for *Conf#6*. Grating lobes for $n = 1, 2, 3, 4, 5$ are plotted with continuous, dashed, and dotted lines. Dark gray continuous line is the grating lobe ($n = 1$) related to the periodicity T of the resistive unit cell. Plot is normalized to its maximum value (10.6 dBsm).

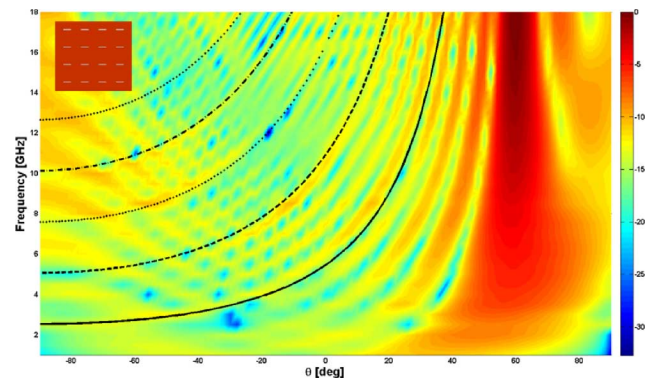

Fig. 24. Normalized scattered field for an impinging TM^y plane wave ($\theta = 60°$) for the original slot array. Grating lobes for $n = 1, 2, 3, 4, 5$ are plotted with continuous, dashed, and dotted lines. Plot is normalized to its maximum value (17.2 dBsm).

directions. The result shown in Fig. 26 assesses the good absorption rate of the structure also for off-normal probing.

B. Monostatic Radar Cross Section

A further aspect that needs to be taken into account consists of looking at monostatic RCS for oblique incidence. Since we have investigated the monostatic RCS of a finite structure, the

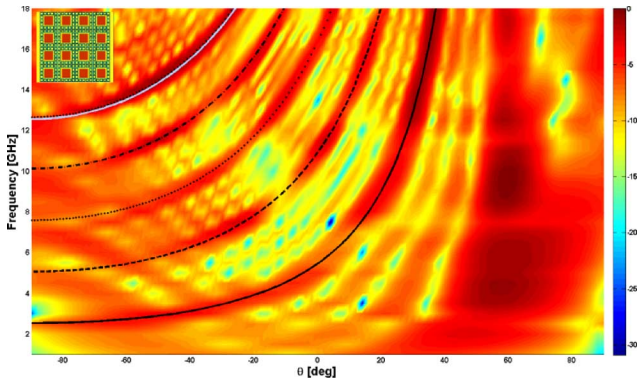

Fig. 25. Normalized scattered field for an impinging TM^y plane wave ($\theta = 60°$) for *Conf#6*. Grating lobes for $n = 1, 2, 3, 4, 5$ are plotted with continuous, dashed, and dotted lines. Dark gray continuous line is the grating lobe ($n = 1$) related to the periodicity T of the resistive unit cell. Plot is normalized to its maximum value (6.5 dBsm).

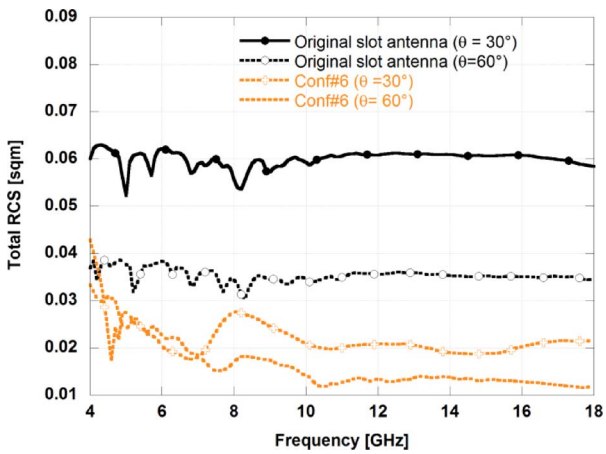

Fig. 26. Comparison between the total RCS in the case of original slot array and *Conf#6* configurations for an impinging TM^y plane wave ($\theta = 30°$ or $\theta = 60, \phi = 180°$).

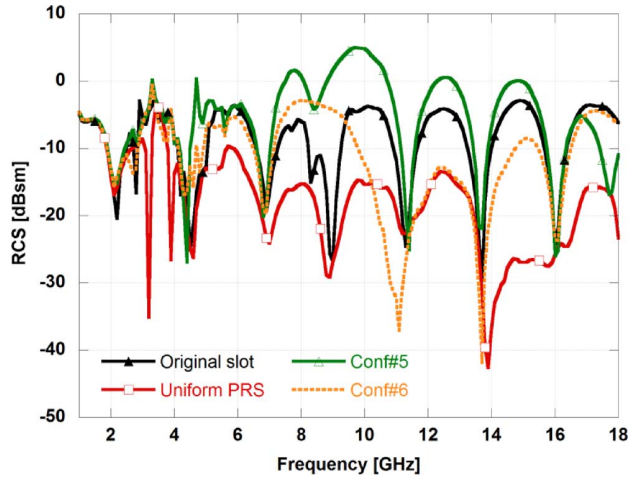

Fig. 27. Comparison among the monostatic RCS of different configurations for an oblique impinging plane wave with TM^y polarization ($\theta = 15°$).

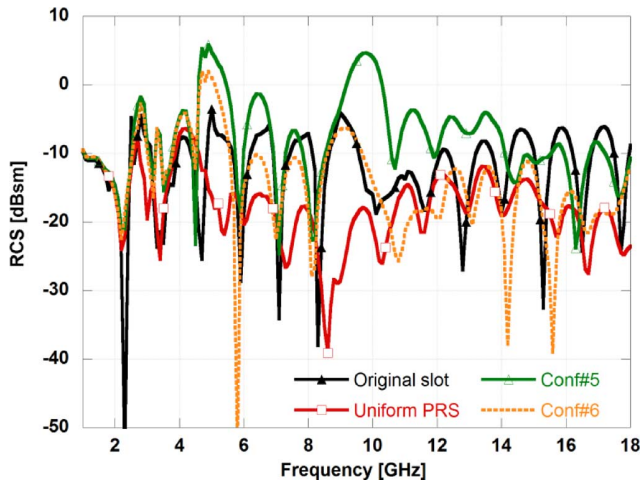

Fig. 28. Comparison among the monostatic RCS of different configurations for an oblique impinging plane wave with TM^y polarization ($\theta = 30°$).

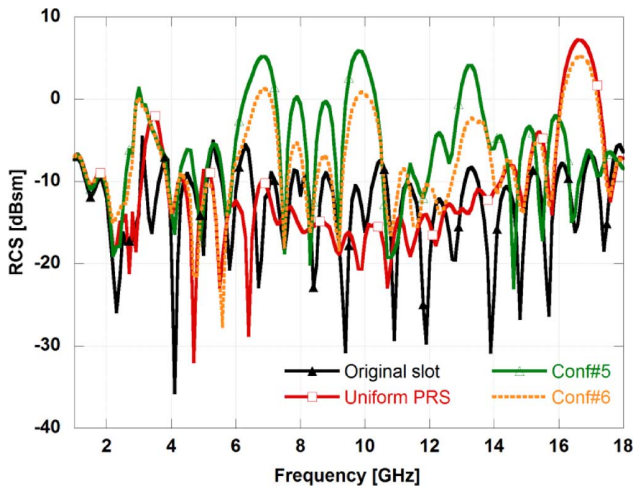

Fig. 29. Comparison among the monostatic RCS of different configurations for an oblique impinging plane wave with TM^y polarization ($\theta = 45°$).

scattered fields due to edge diffractions is clearly present [31]. This contribution depends on the dimension of the considered antenna and it can be mitigated by using resistive cards [32].

The effect of the slot/antenna periodicity P_x and of the resistive pattern T is more general, and it is interesting to evaluate its impact on the RCS of the proposed arrays.

Therefore, we have considered four different directions for a TM^y impinging wave ($\theta = 15°$, $\theta = 30°$, $\theta = 45°$, and $\theta = 60°$) for providing an estimate of the RCSR that a superstrate can achieve under this plane wave illumination. The results are shown in Figs. 27–30. The uniform PRS superstrate guarantees a monostatic RCS lower than the original slot array almost in all cases with the exception at higher frequencies for $\theta = 45°$ and $\theta = 60°$ where PRS grating lobes come into visible range. More in detail, for $\theta = 60°$, the *uniform PRS* configuration exhibits a peak in the monostatic RCS due to the onset of the grating lobes at 13.8 GHz (Fig. 24), whereas *Conf#6* also suffers the emerging of the grating lobe due to the resistive unit cell periodicity (Fig. 25). The *Conf#5* superstrate seems the most critical case since it does not offer a lower monostatic RCS than the original array. This is due to the parasitic metallic elements which enhance the backscattering without absorbing the energy of the incoming wave. The *Conf#6* exhibits an interesting tradeoff since for $\theta = 15°$ and $\theta = 30°$, it provides a radar signature lower than the original array starting from 9

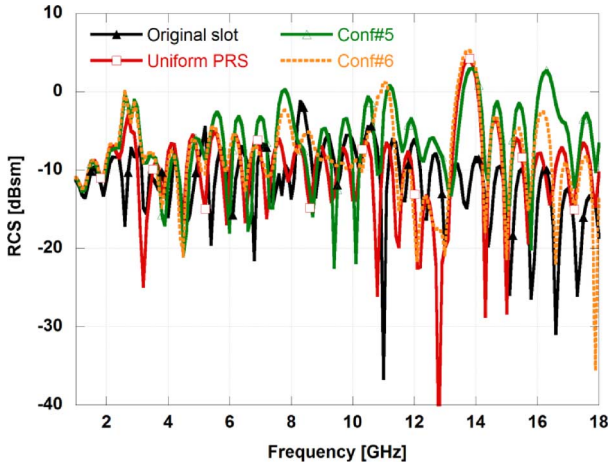

Fig. 30. Comparison among the monostatic RCS of different configurations for an oblique impinging plane wave with TM^y polarization ($\theta = 60°$).

up to 18 GHz. For greater incidence angles, the rise of grating lobes affects the RCS at the frequencies stated by (1). It is clear that absorbing materials are effective in reducing grating lobes generated by the slot/patch periodicity (see also Fig. 16(a)). The only drawback introduced by the presence of the superstrate is the grating lobe due to the periodicity T of the resistive ring, which is located around 17 GHz at 45° and around 14 GHz at 60° incidence.

VII. Conclusion

A microstrip slot array has been presented as a test case to illustrate a strategy for enhancing the performance of the radiating device in terms of RCSR and gain. It has been shown that it is possible to achieve a wideband reduction of the radar signature of an antenna array by properly designing a periodic resistive surface placed as a superstrate to the original array. It has been highlighted that the use of parasitic elements, or the removal of some resistive elements, determines a gain enhancement but also causes some fluctuations in the monostatic RCS due to the onset of grating lobes. A color plot reporting the variation of the scattered field for different angles and frequencies has been introduced with the aim to provide a clear visualization of the energy spread and the grating lobes.

Some of the described solutions guarantee a monostatic RCSR over a two octaves frequency band for normal incidence for both polarizations. Similar performances are exhibited for the bistatic case up to 60°, whereas satisfying results have also been found also for the monostatic RCS for oblique incidence even if in a smaller angular range.

All the presented results and considerations can be useful for designing low-RCS antenna arrays even if different dielectric stackups and periodicities are employed.

References

[1] P. V. Nikitin, K. V. S. Rao, and R. D. Martinez, "Differential RCS of RFID tag," *Electron. Lett.*, vol. 43, no. 8, pp. 431–432, 2007.
[2] E. F. Knott, J. F. Shaeffer, and M. T. Tuley, *Radar Cross Section*. Raleigh, NC, USA: SciTech Pub., 2004.
[3] C. B. Wilsen, D. B. Davidson, J. W. Odendaal, and D. J. Janse van Rensburg, "The RCS reduction of microstrip patch antennas," in *Proc. 10th Int. Conf. Antennas Propag.*, 1997, vol. 1, pp. 174–177.
[4] "Defence Critical Technologies," Joint U.S. Defense Science Board and U.K. Defence Scientific Advisory Council, Task Force on Defence Critical Technologies, Mar. 2006.
[5] J. D. Kraus and R. J. Marhefka, *Antennas*. New York, NY, USA: McGraw–Hill, 2002.
[6] W. Jiang, Y. Liu, S. Gong, and T. Hong, "Application of bionics in antenna radar cross section reduction," *Antennas Wireless Propag. Lett.*, vol. 8, pp. 1275–1278, 2009.
[7] D. D. Reuster, G. A. Thiele, and P. W. Eloe, "Development of low RCS reflector antenna systems," in *Proc. IEEE Antennas Propag. Symp.*, 1994, vol. 3, pp. 2325–2328.
[8] B. A. Munk, *Frequency Selective Surfaces, Theory and Design*. New York, NY, USA: Wiley, 2000.
[9] N. Misran, R. Cahill, and V. F. Fusco, "RCS reduction technique for reflectarray antennas," *Electron. Lett.*, vol. 39, pp. 1630–1631, 2003.
[10] W.-T. Wang, S.-X. Gong, X. Wang, H.-W. Yuan, J. Ling, and T.-T. Wan, "RCS reduction of array antenna by using bandstop FSS reflector," *J. Electrom. Waves Appl.*, vol. 23, no. 11, pp. 1505–1514, 2009.
[11] S. Genovesi, F. Costa, and A. Monorchio, "Low profile array with reduced radar cross section by using hybrid frequency selective surfaces," *IEEE Trans. Antennas Propag.*, vol. 60, no. 5, pp. 2327–2335, 2012.
[12] P. Y. Ufimtsev, "Comments on diffraction principles and limitations of RCS reduction techniques," *Proc. IEEE*, vol. 84, no. 12, pp. 1830–1851, 1996.
[13] H. D. Griffiths, A. J. Garnett, C. J. Baker, and S. Keaveney, "Bistatic radar using satellite-borne illuminators of opportunity," in *Proc. Int. Conf. Radar*, 1992, pp. 276–279.
[14] Y. Li, H. Zhang, Y. Fu, and N. Yuan, "RCS reduction of ridged waveguide slot antenna array using EBG radar absorbing material," *IEEE Antennas Wireless Propag. Lett.*, vol. 7, pp. 473–476, 2008.
[15] D. M. Pozar, "RCS reduction for a microstrip antenna using a normally biased ferrite substrate," *IEEE Microw. Guided Wave Lett.*, vol. 2, no. 5, pp. 196–198, 1992.
[16] F. Costa, S. Genovesi, and A. Monorchio, "A frequency selective absorbing ground plane for low-RCS microstrip antenna arrays," *Progr. Electromagn. Res.*, vol. 126, pp. 317–332, 2012.
[17] H. K. Jang, J. H. Shin, and C. G. Kim, "Low RCS patch array antenna with electromagnetic bandgap using a conducting polymer," in *Proc. Int. Conf. Electromagn. Adv. Appl. (ICEAA)*, Sep. 20–24, 2010, pp. 140–143.
[18] F. Costa and A. Monorchio, "A frequency selective radome with wideband absorbing properties," *IEEE Trans. Antennas Propag.*, vol. 60, no. 6, pp. 2740–2747, 2012.
[19] J. L. Volakis, A. Alexanian, and J. M. Lin, "Broadband RCS reduction of rectangular patch by using distributed loading," *Electron. Lett.*, vol. 28, no. 25, pp. 2322–2323, 1992.
[20] M. Gustafsson, "RCS reduction of integrated antenna arrays and radomes with resistive sheets," in *Proc. IEEE Antennas Propag. Symp.*, Jul. 2006, pp. 3479–3482.
[21] W. Wiesbeck and E. Heidrich, "Influence of antennas on the radar cross section of camouflaged aircraft," in *Proc. Int. Conf. Radar*, 1992, pp. 122–125.
[22] R. B. Green, "The general theory of antenna scattering," Ph.D. dissertation, The Ohio State Univ., Columbus, OH, USA, 1963.
[23] J. A. McEntee, "A technique for measuring the scattering aperture and absorption aperture of an antenna," Tech. Rep., 1957 [Online]. Available: http://handle.dtic.mil/100.2/ADA402379
[24] R. C. Hansen, "Relationship between antennas as scatterers and as radiators," *Proc. IEEE*, vol. 77, no. 5, pp. 659–662, May 1989.
[25] CST Microwave Studio [Online]. Available: http://www.cst.com/Content/Products/MWS/Overview.aspx
[26] F. Costa, S. Genovesi, and A. Monorchio, "On the bandwidth of high-impedance frequency selective surfaces," *IEEE Antennas Wireless Propag. Lett.*, vol. 8, pp. 1341–1344, 2009.
[27] S. Maci, M. Caiazzo, A. Cucini, and M. Casaletti, "A pole-zero matching method for EBG surfaces composed of a dipole FSS printed on a grounded dielectric slab," *IEEE Trans. Antennas Propag.*, vol. 53, no. 1, pp. 70–81, Jan. 2005.
[28] Y. E. Erdemli, K. Sertel, R. A. Gilbert, D. E. Wright, and J. L. Volakis, "Frequency-selective surfaces to enhance performance of broad-band reconfigurable arrays," *IEEE Trans. Antennas Propag.*, vol. 50, no. 12, pp. 1716–1724, Dec. 2002.

[29] F. Costa, A. Monorchio, and G. Manara, "Analysis and design of ultra thin electromagnetic absorbers comprising resistively loaded high impedance surfaces," *IEEE Trans. Antennas Propag.*, vol. 58, no. 5, pp. 1551–1558, 2010.
[30] A. K. Bhattacharyya and D. L. Sengupta, *Radar Cross Section Analysis & Control*. Norwood, MA, USA: Artech House, 1991.
[31] A. E. Culhaoglu, A. V. Osipov, and P. Russer, "Mono- and bistatic scattering reduction by a metamaterial low reflection coating," *IEEE Trans. Antennas Propag.*, vol. 61, no. 1, pp. 462–466, 2013.
[32] D. Lynch, *Introduction to RF Stealth*. Raleigh, NC, USA: SciTech Publishing, 2004.

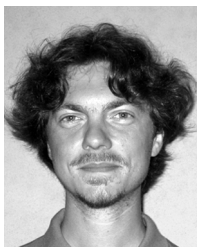

Simone Genovesi (S'99–M'07) received the Laurea degree in telecommunication engineering and the Ph.D. degree in information engineering from the University of Pisa, Pisa, Italy, in 2003 and 2007, respectively.

Since 2003, he has been collaborating with the Electromagnetic Communication Laboratory, Pennsylvania State University (Penn State), University Park, PA, USA. From 2004 to 2006, he has been a Research Associate at the ISTI institute of the National Research Council of Italy (ISTI-CNR), Pisa, Italy. He is currently an Assistant Professor at the Microwave and Radiation Laboratory, University of Pisa. His research focuses on metamaterials, antenna optimization, and evolutionary algorithms.

Filippo Costa (S'07–M'10) was born in Pisa, Italy, on October 31, 1980. He received the M.Sc. degree in telecommunication engineering and the Ph.D. degree in applied electromagnetism in electrical and biomedical engineering, electronics, smart sensors, and nano-technologies from the University of Pisa, Pisa, Italy, in 2006 and 2010, respectively.

From March to August 2009, he was a Visiting Researcher at the Department of Radio Science and Engineering, Helsinki University of Technology (TKK, now Aalto University), Finland. Since January 2010, he has been a Postdoctoral Researcher at the University of Pisa. His research focuses on the analysis and modeling of frequency-selective surfaces and artificial impedance surfaces with emphasis to their application in electromagnetic absorbing materials, antennas, radomes, radio frequency identification, waveguide filters, and techniques for retrieving dielectric permittivity of materials.

Dr. Costa was recipient of the Young Scientist Award of the URSI International Symposium on Electromagnetic Theory in 2013.

Agostino Monorchio (S'89–M'96–SM'04–F'12) received the Laurea degree in electronics engineering and the Ph.D. degree in methods and technologies for environmental monitoring from the University of Pisa, Pisa, Italy, in 1991 and 1994, respectively.

During 1995, he joined the Radio Astronomy Group, Arcetri Astrophysical Observatory, Florence, Italy, as a Postdoctoral Research Fellow, in the area of antennas and microwave systems. He has been collaborating with the Electromagnetic Communication Laboratory, Pennsylvania State University (Penn State), University Park, PA, USA, and he is an Affiliate of the Computational Electromagnetics and Antennas Research Laboratory. He has been a Visiting Scientist at the University of Granada, Spain, and at the Communication University of China, Beijing. In 2010, he affiliated with the Pisa Section of INFN, the National Institute of Nuclear Physics. He is currently an Associate Professor in the School of Engineering, University of Pisa, and Adjunct Professor at the Italian Naval Academy of Livorno. He is also an Adjunct Professor in the Department of Electrical Engineering, Penn State. He is on the Teaching Board of the Ph.D. course in remote sensing and on the council of the Ph.D. School of Engineering "Leonardo da Vinci" at the University of Pisa. He is active in a number of areas, including computational electromagnetics, microwave metamaterials, antennas and radio propagation for wireless networks, active antennas, and electromagnetic compatibility.

Dr. Monorchio has been a reviewer for many scientific journals and he has been supervising numerous research projects related to applied electromagnetic, commissioned and supported by national companies and public institutions. He has served as Associate Editor of the IEEE ANTENNAS AND WIRELESS PROPAGATION LETTERS. He received a Summa Foundation Fellowship and a NATO Senior Fellowship.